Differential cross sections for plasmon excitations and reflected electron-energy-loss spectra

C. J. Tung
Department of Nuclear Science, National Tsing Hua University, Hsinchu, Taiwan

Y. F. Chen and C. M. Kwei
Department of Electronics Engineering, National Chiao Tung University, Hsinchu, Taiwan

T. L. Chou
Department of Nuclear Science, National Tsing Hua University, Hsinchu, Taiwan

(Received 7 June 1993; revised manuscript received 4 March 1994)

Electron differential inverse mean free paths for volume-plasmon excitations and differential probabilities for surface-plasmon excitations have been calculated using dielectric response theory. A model dielectric function which satisfied sum rules and agreed with optical data was established for these calculations. In surface-plasmon calculations, we considered electron-impact emissions of the reflected electron-energy-loss spectroscopy. Formulations were made for obliquely incident electrons with the recoil effect and without the small-scattering-angle assumption. For volume-plasmon excitations, we evaluated corrections due to the exchange and Z_1^3 effects. Comparison between calculated results and experimental data extracted from reflected electron-energy-loss spectra showed good agreement. Calculated differential cross sections have been used to solve the transport equation for the angular and energy flux spectra of reflected electrons. Contributions to the spectra from single and plural plasmon excitations were analyzed. It was found that calculated spectra were in good agreement with measured data.

I. INTRODUCTION

Quantitative information on inelastic interaction cross sections of low-energy electrons in solids is important in surface analysis such as Auger electron spectroscopy, x-ray photoelectron spectroscopy, reflected electron-energy-loss spectroscopy (REELS), etc. Computations of this information require the dielectric response theory[1,2] for electron-solid interactions through, primarily, volume and surface excitations. Alternatively, this information can be extracted from measured REELS spectra.[3-5] The advancement of both theoretical and experimental data on electron inelastic cross sections leads to significant improvements in accurate surface analysis.

In this work, we calculate electron differential inverse free paths (DIMFP's) for volume-plasmon excitations and differential probabilities for surface-plasmon excitations and compare the results with those extracted from measured REELS spectra. Our approach involves the use of a dielectric response theory for inelastic interactions and a Boltzmann equation for electron transport in solids. Some minor effects contributing to the energy losses of low-energy electrons, e.g., the recoil effect in surface excitations and the correlation, exchange and Z_1^3 effects in volume excitations, are included in our theory. Other effects such as the quantal interference between scattered electrons and residual ions, which are negligibly small in the energy range considered in this work, i.e., 300 eV–10 keV, are omitted. A review about the validity and the limitation of dielectric response theory for low-energy electrons is available.[6] A discussion on the applicability of the Boltzmann transport equation to low-energy secondary electrons is also available.[7] The rationale underlying the modeling of the transport of swift electrons in solids was given there. Due to the complex interactions and transport of these electrons, our results seem quite encouraging.

The volume energy-loss function, or the imaginary part of the negative inverse dielectric function, $\mathrm{Im}(-1/\varepsilon)$, was modeled previously[8] as a sum of Drude response function terms. In that model, the leading coefficients were determined by a fit of the energy-loss-function in the optical limit to experimental data. Although Kramers-Kronig transformations[9] may be applied to derive the real part of the dielectric function, ε_1, and the imaginary part of this function, ε_2, these transformations often produce unreliable results due to the incompleteness of measured energy-loss functions over a wide range of energy transfers. Any small errors occurring near the faint humps corresponding to interband transitions in the energy-loss function may result in amplifying errors in the derived ε_1 and ε_2.[10] Thus, the model based on the volume energy-loss function should not be applied to compute the surface energy-loss function where accurate ε_1 and ε_2 over an extended range of energy and momentum transfers are required. To improve this model, Kwei and Tung[11] considered ε_2 as a sum of Drude response terms in a modified approach. They chose to fit ε_2 to experimental data in the optical limit. Then, ε_1 and $\mathrm{Im}(-1/\varepsilon)$ were determined using fitted coefficients. In this work, we further generalize this approach by requiring all fitted critical-point energies to match those identified in interband transitions and by allowing a background dielectric constant to account for the influence of polarizable ion cores.[12] In addition, we require that sum rules for ε_2 and $\mathrm{Im}(-1/\varepsilon)$ are satisfied.

With the present model for dielectric functions, an estimate of surface and volume energy-loss functions can be made more accurately. One can subsequently calculate the DIMFP for volume-plasmon excitations and the differential probability for surface-plasmon excitations. Here we calculate these quantities for swift electrons interacting with several solids and compare our results with data extracted from measured REELS spectra. Since these spectra contain single, plural and multiple scattering energy-loss peaks, they must be deconvoluted in order to separate out individual scattering contributions. This can be done by solving the electron-transport equation under simulated REELS conditions. Our calculations show that the relative importance of surface to volume excitations depends on the solid material and on the electron energy. The calculated results are in good agreement with experimental data.

II. THEORY

A. Plasmon excitations

In REELS, incident electrons interact inelastically with solid electrons in the sample mainly through volume and surface excitations. Solid electrons near the surface are responsible primarily for surface excitations, while those deep inside contribute mostly to volume excitations. Both surface and volume excitations may be described by a complex dielectric function of the sample.

In this paper we use atomic units for quantities and units unless otherwise specified. Considering a swift electron of velocity v impinging on a homogeneous and isotropic solid, the DIMFP of this electron with energy $E=v^2/2$ to lose energy ω for volume excitations is given in the first-Born approximation as[1,13]

$$\mu_v^{(1)}(E\rightarrow E-\omega)=\frac{2}{\pi v^2}\int_{k_-}^{k_+}\frac{1}{k}\mathrm{Im}\left[\frac{-1}{\varepsilon(k,\omega)}\right]dk\ , \tag{1}$$

where k is the momentum transfer and $k_\pm=\sqrt{2E}\pm\sqrt{2(E-\omega)}$ comes from the conservation of energy and momentum. The validity of the first-Born approximation of Eq. (1) has been discussed.[14–17] It was argued that this approximation gave a good estimate of the electron DIMFP for valence-band excitations under the condition $E>7E_F$. In this work, the incident electron energies range from 0.3 to 10 keV and the Fermi energies, E_F, lie in the interval 10–15 eV. Therefore, Eq. (1) should work reasonably well. To estimate the accuracy of this equation, we can apply the second-order Born approximation. Following the derivation in the Z_1^3 effect of the stopping power formula,[18,19] we find

$$\mu_v(E\rightarrow E-\omega)=\mu_v^{(1)}(E\rightarrow E-\omega)+\mu_v^{(2)}(E\rightarrow E-\omega)\ , \tag{2}$$

where

$$\mu_v^{(2)}(E\rightarrow E-\omega)=\frac{-2}{\pi v^2}\mathrm{Im}\left[\frac{-1}{\varepsilon(0,\omega)}\right]L(\omega) \tag{3}$$

is the correction term contributed by the second Born approximation and $L(\omega)=(\omega/v^3)I(\chi\omega/v)$. In this work, we take $\chi=1/\sqrt{2\omega}$ (Ref. 20) and tabulated data for the $I(\chi\omega/v)$.[21]

In the Born approximation, it is assumed that successive interactions between an energetic electron and ions and electrons in the medium are independent. Therefore, a quasiparticle representation may be formed. For a low-energy electron, its mean free path in the solid may be only a few angstroms. Such an electron and its polarization dressing can be so strongly damped that the quasiparticle description may lose its validity. It was evaluated by Quinn[22] that the damping rate was at most 16% for low-energy electrons in aluminum metal. Thus, Ritchie *et al.*[6] have concluded that the quasiparticle concept should be reasonable for low-energy electrons in any electron gas of density comparable to that of the conduction electrons in aluminum. Recently, a theory was determined[23] for the description of elastic and inelastic interactions in terms of quasiparticle representations involving damped one-electron functions. In our model dielectric function, each quasiparticle is characterized by a separate oscillator with its effective mass, bond strength, and damping to be determined by a fit of this function to the optical data. Thus, our treatment is equivalent to the above quasiparticle theory except that we determine characteristic properties experimentally. A detailed discussion about our model dielectric function will be presented in the next section.

The inverse mean free path (IMFP) of an electron for volume excitations is then given by

$$\mu_v(E)=\int_0^E\mu_v(E\rightarrow E-\omega)d\omega\ . \tag{4}$$

Note that we denote DIMFP by double variables separated by an arrow in the parenthesis and IMFP by a single variable within the parenthesis.

The dielectric response theory also provides a description about surface excitations. The differential probability per unit energy loss per unit momentum transfer of an electron for such excitations may be in terms of the dielectric function too. This probability was derived by Ritchie[24] for normal incident electrons through the neglect of the recoil effect. Omitting the same effect, Raether[2] worked out such a probability under the small-scattering-angle approximation for obliquely incident electrons. The present work derives this probability for obliquely incident electrons with the recoil effect and without the small scattering-angle approximation. For a sample of thickness s, we find

$$P_s(E\rightarrow E-\omega,\mathbf{v}\rightarrow\mathbf{v}-\mathbf{k})=\frac{2|k_s|}{\pi^2 v(\cos\alpha)k^4}\times\mathrm{Im}\left[\frac{(\varepsilon-1)^2}{\varepsilon}R_c\right]\times\delta\left[\omega-\mathbf{v}\cdot\mathbf{k}+\frac{k^2}{2}\right] \tag{5}$$

for the differential probability of an electron with energy E to lose energy ω and transfer momentum $\mathbf{k}$ in surface excitations. Here

$$R_c=\frac{\sin^2(s\omega/2v)}{\varepsilon+\tanh(sk_s/2)}+\frac{\cos^2(s\omega/2v)}{\varepsilon+\coth(sk_s/2)}\ , \tag{6}$$

α is the angle between the surface normal and the direction of the incident electron, k_s is the parallel component of momentum transfer along the surface plane, and $\delta(\ )$ denotes the conservation of energy and momentum. In REELS applications, the sample thickness is large enough to reach a saturated surface excitation probability. In such situations, Eq. (5) reduces to

$$P_s(E\to E-\omega,\mathbf{v}\to\mathbf{v}-\mathbf{k})=\frac{2|k_s|}{\pi^2 v(\cos\alpha)k^4}\times\mathrm{Im}\left[\frac{(\varepsilon-1)^2}{\varepsilon(\varepsilon+1)}\right]\times\delta\left[\omega-\mathbf{v}\cdot\mathbf{k}+\frac{k^2}{2}\right]\ . \tag{7}$$

We can decompose $\mathbf{k}$ into $k_\perp$ and $k_\parallel$ corresponding to the perpendicular and parallel components of $\mathbf{k}$ along $\mathbf{v}$. Assuming that the scattering angle θ lies on the plane of the incident electron, as sketched in Fig. 1, we can write

$$k_s=k_\perp\cos\alpha\pm k_\parallel\sin\alpha\ , \tag{8}$$

where the positive (negative) sign is for the like (opposite) signs of θ and α. Carrying out the integration over $\mathbf{k}$ in Eq. (7), we obtain the surface excitation probability per unit energy loss as

$$P_s(E\to E-\omega)=P_{s+}(E\to E-\omega)+P_{s-}(E\to E-\omega)\ , \tag{9}$$

where

$$P_{s\pm}(E\to E-\omega)=\frac{2}{\pi v^2(\cos\alpha)}\int_{k_-}^{k_+}\frac{|k_s'|}{k^3}\mathrm{Im}\left[\frac{(\varepsilon-1)^2}{\varepsilon(\varepsilon+1)}\right]dk \tag{10}$$

and

$$k_s'=\left[k^2-\left[\frac{\omega}{v}+\frac{k^2}{2v}\right]^2\right]^{1/2}\cos\alpha\pm\left[\frac{\omega}{v}+\frac{k^2}{2v}\right]\sin\alpha\ . \tag{11}$$

Since k_s' is different for positive and negative signs in Eq. (11), an asymmetry effect exists in the surface excitation probability with respect to scattering angle orientations. This effect has been confirmed experimentally.[25]

If we neglect the recoil term in Eq. (7) and carry out the integration over $k_\parallel$, we obtain

$$P_{s\perp}(E\to E-\omega\ ,\mathbf{v}\to\mathbf{v}-\mathbf{k})=\frac{2|k_s|}{\pi^2 v^2(\cos\alpha)(k_\perp^2+\omega^2/v^2)^2}\times\mathrm{Im}\left[\frac{(\varepsilon-1)^2}{\varepsilon(\varepsilon+1)}\right] \tag{12}$$

with

$$k_s=k_\perp\cos\alpha\pm\frac{\omega}{v}\sin\alpha\ . \tag{13}$$

Taking $\alpha=0$ in Eq. (12), we find that the result of Ritchie for a normal incident electron is a special case of this equation. Letting $\theta\ll 1$ and $k\ll v$ in Eq. (12), we get the result of Raether for obliquely incident electrons under the small-scattering-angle approximation.

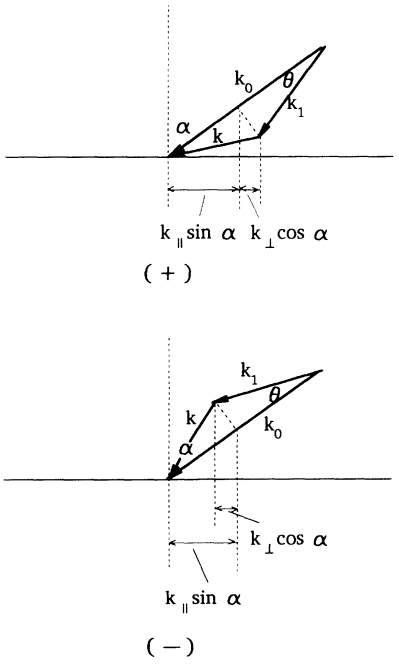

FIG. 1. A sketch of the electron configuration in REELS. Here $\mathbf{k}_0$, $\mathbf{k}_1$, and $\mathbf{k}$ are, respectively, electron momentum before the scattering, electron momentum after the scattering, and the momentum transfer; $k_\perp$ and $k_\parallel$ are, respectively, the perpendicular and parallel components of $\mathbf{k}$ along $\mathbf{k}_0$; α and θ are, respectively, the angle between the surface normal and the electron incident direction and the scattering angle (either positive or negative). The scattering angle is assumed to lie on the plane of incidence.

B. Dielectric functions

The model dielectric function used in this work is an extended Drude model applied to the valence band (or conduction band for metals) of a solid. The real and imaginary parts of the dielectric function are given by[2,26]

$$\varepsilon_1(k,\omega)=\varepsilon_b-\sum_i\frac{A_i[\omega^2-(\omega_i+k^2/2)^2]}{[\omega^2-(\omega_i+k^2/2)^2]^2+\omega^2\gamma_i^2} \tag{14}$$

and

$$\varepsilon_2(k,\omega)=\sum_i\frac{A_i\gamma_i\omega}{[\omega^2-(\omega_i+k^2/2)^2]^2+\omega^2\gamma_i^2}\ , \tag{15}$$

where A_i, γ_i, and ω_i, are, respectively, the oscillator strength, damping coefficient, and critical-point energy, all associated with the ith interband transition. Note that we include in Eq. (14) an ε_b term to account for the background dielectric constant due to the influence of polarizable ion cores.[12] This term can be important at energy transfers just below the threshold energy of inner-shell electrons. Since the exact dependence of the dielectric function on momentum transfer is seldom known, an ex-

trapolation from the optical limit to other momentum transfers must be made. The expression adopted in Eqs. (14) and (15) for the k dependence works correctly at the two ends of the momentum transfer, i.e., $k \rightarrow 0$ and $k \rightarrow \infty$, with an accuracy proportional to k^2.[27] The energy-loss function can then be calculated using

$$\mathrm{Im}\left[\frac{-1}{\varepsilon(k,\omega)}\right]=\frac{\varepsilon_2}{\varepsilon_1^2+\varepsilon_2^2} . \tag{16}$$

Parameters in Eq. (15) will be determined by a fit of this equation, in the limit $k \rightarrow 0$, to the optical dielectric function data taken from energy-loss and optical measurements. These two measurements are often complementary to each other in producing reliable data over a wide range of energy transfers. Generally, optical experiments[28] provide detailed information on interband transitions at small energy transfers. Whereas, energy-loss experiments[29] give accurate data on energy-loss functions at large energy transfers. To ensure the accuracy of fitted parameters, we require that the model dielectric function satisfies two sum rules, i.e.,[12]

$$\int_0^\infty \omega\varepsilon_2(0,\omega)d\omega=\frac{\pi}{2}\sum_i A_i=\frac{\pi}{2}\omega_p^2 \tag{17}$$

and

$$\int_0^\infty \omega\,\mathrm{Im}\left[\frac{-1}{\varepsilon(0,\omega)}\right]d\omega=\frac{\pi\omega_p^2}{2\varepsilon_b^2} , \tag{18}$$

where ω_p is the plasma energy of valence electrons.

Besides plasmon damping and ion polarizability, there are other effects which contribute to the DIMFP of low-energy electrons. These include the local-field corrections[30] due to correlation and exchange. With our model dielectric function fitted to experimental data, the influence of correlation is already incorporated. The exchange correction, arising from the requirement of an antisymmetric wave function for an assembly of electrons under interchange of spin and space coordinates, can be estimated using a semiempirical scheme.[6,31] This scheme is based on the Moller differential cross section.[32] For metals, the exchange-corrected DIMFP is given by

$$\mu_v^{\mathrm{ex}}(E\rightarrow E-\omega)=\mu_v(E\rightarrow E-\omega)+\mu_v(E\rightarrow\omega) -[\mu_v(E\rightarrow E-\omega)\mu_v(E\rightarrow\omega)]^{1/2} . \tag{19}$$

Additional modifications to the DIMFP of very low-energy electrons, such as the quantal interference between scattered electrons and residual ions, have been discussed by Ritchie *et al.*[6] Since these modifications are negligibly small for electrons in the energy range of current interest, we can omit them in this work.

C. REELS spectra

As illustrated in Fig. 2, an incident electron of energy E_0 and direction Ω_0 travels the zigzag trajectory inside a solid before it is reflected back to vacuum with energy E and direction Ω. Elastic and inelastic interactions contribute mainly to, respectively, the angular deflection and the energy loss of this electron. Inelastic interactions

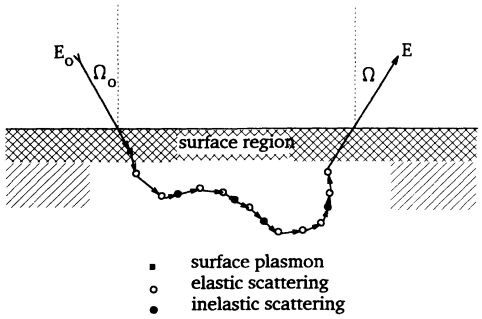

FIG. 2. A sketch of the zigzag trajectory of an electron inside the solid for REELS simulations.

consist of single-electron excitations (interband transitions) and ionizations, volume-plasmon excitations, and surface-plasmon excitations. To get an idea of how these interactions occur in the solid, we consider, as an example, the reflection of a 500-eV electron from aluminum. In this case, the mean pathlength traveled by the electron, the elastic mean free path, and the inelastic mean free path (excluding surface-plasmon excitations) are about[3,30,33] 125, 5.8, and 12.4 Å, respectively. Therefore, the average number of elastic and inelastic interactions in the solid are about 22 and 10. For surface-plasmon excitations, the effective region extends into the solid to a depth about v/ω_s,[1] where ω_s is the surface-plasmon frequency. Since $\omega_s \approx 10$ eV,[3] this depth is around 9 Å, sufficient only for a single surface-plasmon excitation. It can be predicted that multiple surface plasmons are unlikely to occur for a normally incident electron. Only when the electron makes a very large glancing angle, plural surface plasmons can be possible. This conclusion agrees with experimental observations.[34]

The starting point for a theoretical description of electron angular and energy flux distribution in REELS is the Bolzmann transport equation. This equation represents a continuity relation in phase space, which is made up of coordinates $\mathbf{r}$, the kinetic energy E, and the direction of motion Ω, of the transport electron. The mathematical formulation for the energy and angular electron flux at time t is given by

$$\left[\frac{\partial}{\partial t}+\nabla\cdot\Omega\right]\phi(\mathbf{r},E,\Omega,t) = S(\mathbf{r},E,\Omega,t) + \int\int\phi(\mathbf{r},E',\Omega',t)\mu(E'\rightarrow E,\Omega'\rightarrow\Omega)dE'd\Omega' - \int\int\phi(\mathbf{r},E,\Omega,t)\mu(E\rightarrow E',\Omega\rightarrow\Omega')dE'd\Omega' , \tag{20}$$

where $S(\mathbf{r},E,\Omega,t)$ is the number of source electrons per unit volume, solid angle, and energy at time t. The double DIMFP, $\mu(E'\rightarrow E,\Omega'\rightarrow\Omega)$, is the probability per unit pathlength, energy, and solid angle that an electron of initial energy E' and direction Ω' reaches the final energy E and direction Ω.

In general, it is difficult to solve Eq. (20) because of the

energy-angle correlating DIMFP involved in this equation. However, it is reasonable to assume that[35] only elastic interactions contribute to the angular deflection and only inelastic interactions contribute to the energy loss. Hence, one may separate the DIMFP according to

$$\mu(E'\to E,\Omega'\to\Omega)=\mu_e(\Omega'\to\Omega)\delta(E'-E)+\mu_i(E'\to E)\delta(\Omega'-\Omega)\ , \quad (21)$$

where μ_e and μ_i are, respectively, elastic and inelastic DIMFP's. For the moment, we consider μ_i in Eq. (21) consisting of volume-plasmon excitations and interband transitions but not of surface-plasmon excitations. One may decouple the electron flux into angular and energy parts according to

$$\phi(\mathbf{r},E,\Omega,t)=Q(\mathbf{r},\Omega,t)G(\mathbf{r},E,t)\ . \quad (22)$$

Assuming an azimuthal symmetry for REELS and defining $\eta=\cos\theta$ and $R=vt$, one obtains

$$\left[\frac{\partial}{\partial R}+\eta\frac{\partial}{\partial x}\right]Q(x,\eta,R)=\delta(x)\delta(\eta-\eta_0)\delta(R)+\int Q(x,\eta',R)\mu_e(\eta'\to\eta)d\eta'-\int Q(x,\eta,R)\mu_e(\eta\to\eta')d\eta' \quad (23)$$

for the angular distribution function at depth x and path-length R and

$$\frac{\partial}{\partial R}G(x,E,R)=\delta(x)\delta(E-E_0)\delta(R)+\int G(x,E',R)\mu_i(E'\to E)dE'-\int G(x,E,R)\mu_i(E\to E')dE' \quad (24)$$

for the corresponding energy distribution function.

The solution of Eq. (23) may be found by expanding the angular distribution function in terms of the Legendre polynomial. It gives[36]

$$Q(0,\eta,R)=A(\eta_0,\eta)\lambda_t^{-1}e^{-R/L}\ , \quad (25)$$

where λ_t is the transport elastic mean free path, $L\approx 2\lambda_t$ is the attenuation length, and $A(\eta_0,\eta)$ depends on the directional cosines of incident and exit angles of the electron.

To find the time integral of the energy and angular distribution flux, one defines

$$\phi(0,E,\eta)=\int_0^\infty Q(0,\eta,R)G(0,E,R)dR\ . \quad (26)$$

This flux can be determined by multiplying Eq. (24) by $Q(0,\eta,R)$ and integrating the result over R. Combining it with Eqs. (25) and (26), we find

$$\frac{A(\eta_0,\eta)}{\lambda_t}\delta(E-E_0)=\frac{\lambda_i+L}{\lambda_i L}\phi(0,E,\eta)-\int\phi(0,E',\eta)\mu_i(E'\to E)dE'\ , \quad (27)$$

where λ_i is the electron inelastic mean free path. Equation (24) could also be derived by assuming a Landau distribution for $G(0,E,R)$.[3] The present derivation, however, does not resort to such an energy distribution. Defining a relative electron flux-density distribution as

$$f(0,E,\eta)=\frac{\lambda_t}{A(\eta_0,\eta)}\frac{\lambda_i+L}{\lambda_i L}\phi(0,E,\eta)\ , \quad (28)$$

one gets

$$f(0,E,\eta)=\delta(E-E_0)+\frac{\lambda_i L}{\lambda_i+L}\int\mu_i(E'\to E)f(0,E',\eta)dE'\ . \quad (29)$$

If we neglect elastic scatterings in Eq. (29), i.e., assuming $L\gg\lambda_i$, the leading factor on the right-hand side (RHS) becomes λ_i^{-1}. Thus, this equation reduces to the common transport equation for an electron slowing-down spectrum due to inelastic interactions.[37] On the other hand, if we assume $L\ll\lambda_i$, the leading factor on the RHS of Eq. (29) becomes L^{-1}. Then, the energy spectrum in REELS is modified by elastic scatterings.

If only small energy losses are concerned, Eq. (29) may be solved by an iteration process. One obtains

$$f(0,E,\eta)=\delta(E-E_0)+\frac{\lambda_i L}{\lambda_i+L}\mu_i(E_0\to E)+\left[\frac{\lambda_i L}{\lambda_i+L}\right]^2\int\mu_i(E_0\to E')\times\mu_i(E'\to E)dE'+\cdots\ , \quad (30)$$

where the first, second, and third terms on the RHS represent, respectively, electron-energy-loss flux due to zero, single, and double inelastic interactions. So far, we have excluded the contribution from surface excitations in Eq. (30) because it required a different treatment. Surface excitations are characterized not by a DIMFP but by a differential probability. Their occurrence follows a description of the Poisson statistics.[1] Thus, we may include these excitations to Eq. (30) by the replacement of

$$\frac{\lambda_i L}{\lambda_i+L}\mu_i(E'\to E)$$

with $K'(E'\to E)$, where

$$K'(E'\to E)=\frac{\lambda_i L}{\lambda_i+L}\mu_i(E'\to E)+P_s(E'\to E)\ . \quad (31)$$

In order to compare with the effective inelastic-scattering cross section defined in Ref. 3, we let $K(E'\to E)$ be the normalized function of $K'(E'\to E)$. Explicitly, we may write the transport equation for REELS spectra as

$$f(0,E,\eta)=\delta(E-E_0)+P_s(E_0\to E)+\frac{\lambda_i L}{\lambda_i+L}\mu_i(E_0\to E)$$
$$+\frac{\lambda_i L}{\lambda_i+L}\int[P_s(E_0\to E')\mu_i(E'\to E)+\mu_i(E_0\to E')P_s(E'\to E)]dE'$$
$$+\left[\frac{\lambda_i L}{\lambda_i+L}\right]^2\int\mu_i(E_0\to E')\mu_i(E'\to E)dE'+\int P_s(E_0\to E')P_s(E'\to E)dE'+\cdots . \quad (32)$$

Here we label contributions from the first, second, third, etc., terms on the RHS of Eq. (32) by 0, 1s, 1v, 1sv, 2v, etc. In Fig. 3, we plot the results of measured REELS spectrum for an electron of 2 keV energy and 25° incident angle in Al.[3] It is clearly seen that strong peaks in the spectrum correspond to zero plasmon, a surface plasmon, a volume plasmon, a surface plasmon and a volume plasmon, and two volume plasmons, etc. The lack of a peak at ~20 eV indicates that the probability of plural surface-plasmon excitations is negligibly small. This confirms the discussion presented previously. For solids of a broader energy-loss function, the identification of individual plasmon contributions could be difficult due to the overlapping of plasmon peaks in the spectrum.

III. RESULTS AND DISCUSSION

Tables I and II list parameters in the model dielectric function obtained by a fit of Eq. (15), in the limit of $k\to 0$, to optical data for Fe,[38,39] Pd,[40–42] Cu,[43–45] and Au.[45] In these fits, we check not only the accuracy of $\varepsilon_1(0,\omega)$, $\varepsilon_2(0,\omega)$, and $\mathrm{Im}[-1/\varepsilon(0,\omega)]$ determined by Eqs. (14)–(16) but also the extent to which they satisfy the sum rules of Eqs. (17) and (18). Furthermore, we require that the total valence oscillator strength, i.e., $\sum_i A_i$, agrees with the prediction from observed plasmon energies.[1] Figure 4 shows a comparison of $\varepsilon_1(0,\omega)$, $\varepsilon_2(0,\omega)$, and $\mathrm{Im}[-1/\varepsilon(0,\omega)]$ for Fe calculated presently (solid curves) and determined experimentally (dashed curves). It is seen that good agreement is found between present results and experiment data for all functions plotted. For Fe, Cu, and Au, our fits cover the loosely bound inner shells due to the overlapping of oscillator strengths between the valence band and these shells in the vicinity of their binding energies.

Based on the model dielectric function, we have calculated the DIMFP for volume-plasmon excitations. Figure 5 shows the results of these calculations for a 500-eV electron in Cu. It is seen that the second Born approximation reduces the DIMFP of the first Born approximation by a tiny amount at all energy losses. This reduction becomes even smaller for higher-energy electrons. It will have little effect on the resulting REELS spectra. The exchange effect further decreases the DIMFP by also a small amount. At any rate, we have incorporated the second Born approximation and the exchange effect in our calculations. Figure 6 shows the results of the DIMFP for volume excitations, the differential probability for surface excitations, and the sum of these two quantities for electrons with various energies in Fe. Here we took $\alpha=20°$ for surface calculations in order to compare our results with data extracted from REELS spectra.[4] It is revealed that the contribution from volume excitations

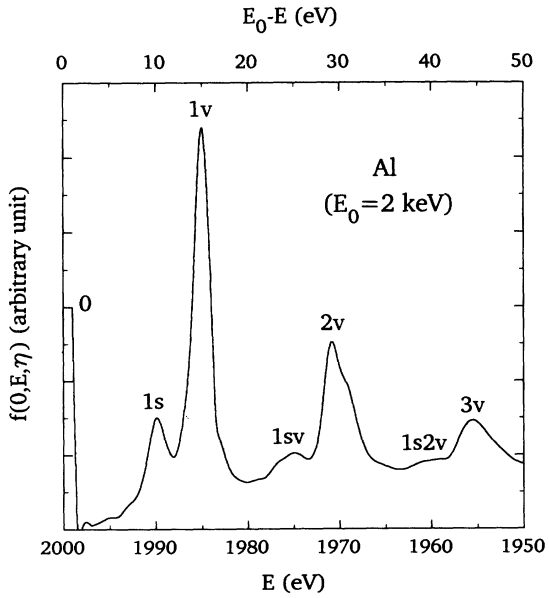

FIG. 3. The identification of individual contributions from surface- and volume-plasmon excitations to the measured REELS spectrum for a 2-keV electron in Al (Ref. 3). Here 0, 1s, 1v, 1sv, etc. denote zero plasmon, a surface plasmon, a volume plasmon, a surface and a volume plasmon, etc.

TABLE I. Parameters in the model dielectric function of Eq. (15) for Fe and Pd.

Fe $\varepsilon_b=1.12$			Pd $\varepsilon_b=1.00$		
A_i (eV^2)	γ_i (eV)	ω_i (eV)	A_i (eV^2)	γ_i (eV)	ω_i (eV)
40	0.118	0	85	0.1	0
30	2	0.45	75	4.45	1.3
50	4	1.5	45	4.45	4.3
130	6	3.2	45	5	10.7
10	2	6.04	2	0.7	11.8
41.4	4.8	9.56	13	1.8	13.65
28	3.2	12.9	45	3	15
300	18	20	50	4.6	16.8
60	30	48	110	5.6	20.5
190	10	58	80	6	24.2
993	100	84	70	7	30.6
			130	17	38
			186	19	49

TABLE II. Parameters in the model dielectric function of Eq. (15) for Au and Cu.

Cu $\varepsilon_b=1.05$			Au $\varepsilon_b=1.00$		
A_i (eV^2)	γ_i (eV)	ω_i (eV)	A_i (eV^2)	γ_i (eV)	ω_i (eV)
64	0.03	0	79	0.1	0
6	0.3	0.3	9	1	3.1
6.5	0.65	2.5	36	1.9	4.1
5.5	0.7	3.1	17	2.3	5.3
4	0.7	3.7	60	4	8.17
55	2.6	5.05	100	9	12
42	4.76	8.93	120	10	14
172	10.18	14.74	155	6	21.3
80	8	25.6	145	7.2	29.5
240	32	40	280	20	38.5
90	30	55	360	28	63
85	30	65	183	26	100
200	25	83			
500	65	120			
664	160	200			

increases with electron energy. The contribution from surface excitations, however, dominates at small energy losses for, especially, low-energy electrons. This domination gradually turns over to volume excitations as electron energy becomes greater. In all cases, the agreement between calculated results (solid curves) and experimental data (dashed curves) is good over a wide range of electron energies and energy losses. A similar plot of these results for electrons in Pd is shown in Fig. 7. Again, we took $\alpha=20°$ for surface calculations. In this case, the surface plasmon peaks are steeper and narrower than the volume plasmon peaks.

Figure 8 shows a comparison of $K(E'\rightarrow E)$ calculated presently (solid curve), extracted from measured REELS

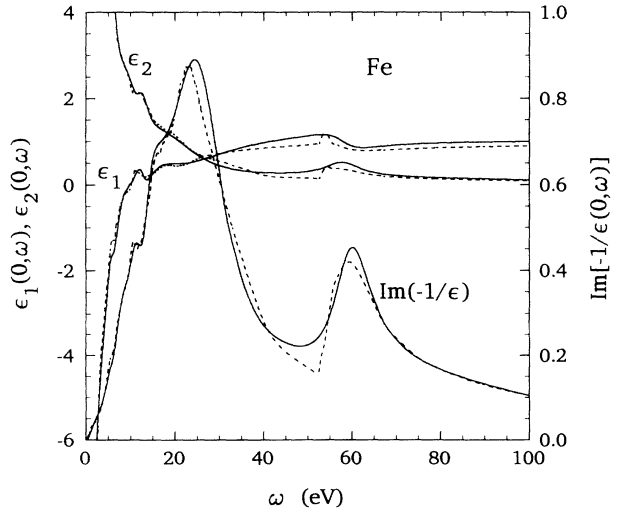

FIG. 4. A comparison of experimental data (dashed curves) (Refs. 38 and 39) and calculated results (solid curves) on the real part of the dielectric function $\varepsilon_1(0,\omega)$, the imaginary part of the dielectric function $\varepsilon_2(0,\omega)$, and the energy-loss function $\mathrm{Im}[-1/\varepsilon(0,\omega)]$ for Fe.

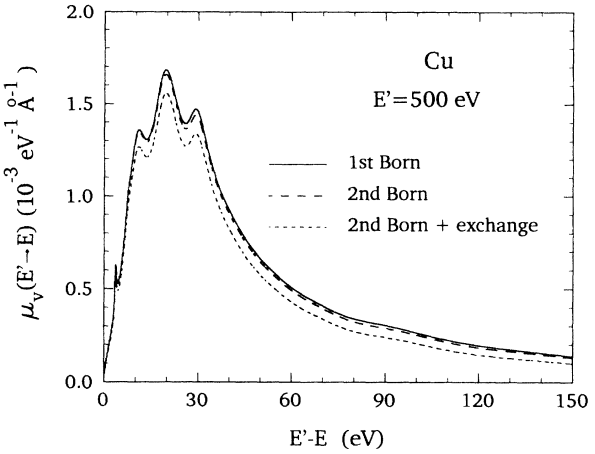

FIG. 5. The differential inverse mean free path of a 500-eV electron in Cu. The first Born approximation, Eq. (1), the second Born approximation, Eqs. (2) and (3), and the exchange effect, Eq. (19), are used for calculations.

spectra (dashed curve),[4] and determined using two different models (chain curves) (Ref. 5) for a 300-eV electron in Au. It is shown that the agreement of REELS data with present results is better than that with other

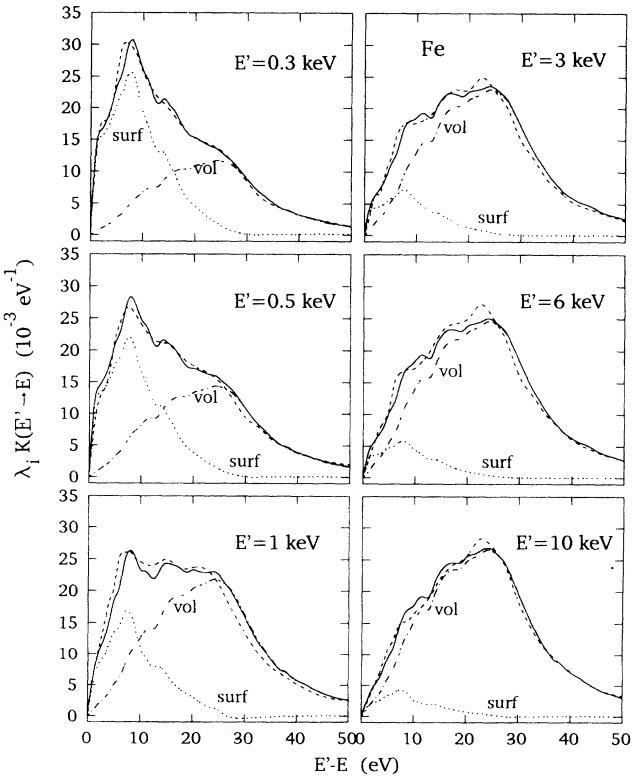

FIG. 6. A plot of the differential scattering probability for electrons with different energies in Fe. The dashed, dotted, chain and solid curves, are, respectively, data extracted from measured REELS spectra,[4] calculated results of the surface excitation probability, calculated results of the volume excitation probability, and calculated results of the total excitation probability.

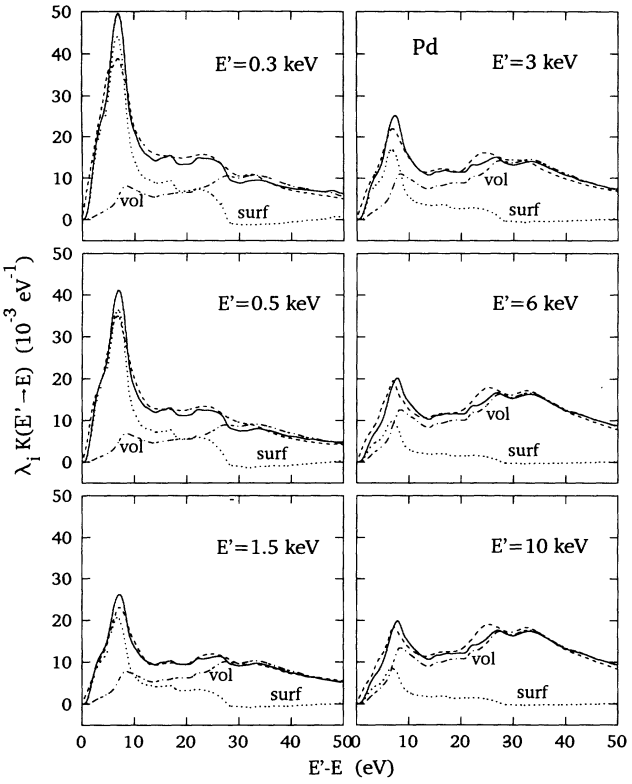

FIG. 7. A plot of the differential scattering probability for electrons with different energies in Pd. The dashed, dotted, chain and solid curves, are, respectively, data extracted from measured REELS spectra (Ref. 4), calculated results of the surface excitation probability, calculated results of the volume excitation probability, and calculated results of the total excitation probability.

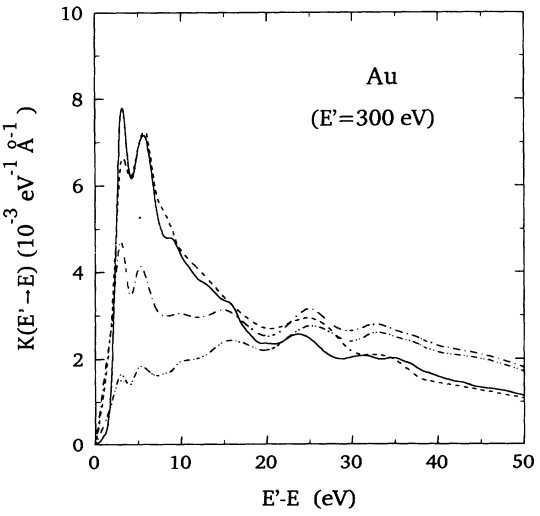

FIG. 8. A plot of the differential probability for a 300-eV electron in Au. The chain, dashed, and solid curves are, respectively, results of two model calculations (Ref. 5), data extracted from measured REELS spectra (Ref. 4) and present results.

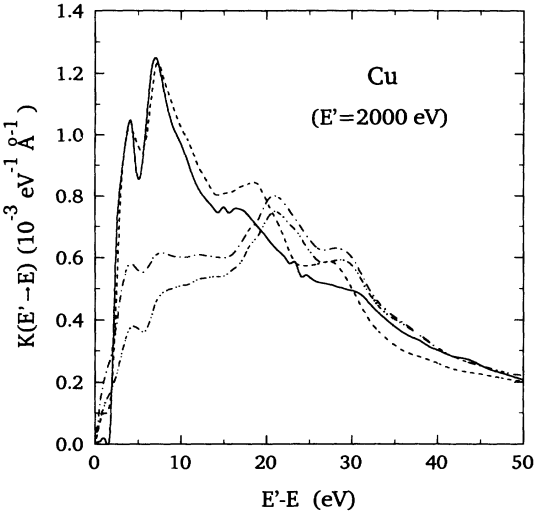

FIG. 9. A plot of the differential probability for a 2-keV electron in Cu. The chain, dashed, and solid curves are, respectively, results of two model calculations (Ref. 5), data extracted from measured REELS spectra (Ref. 4) and present results.

model calculations. Once again, surface excitations contribute strongly at small energy losses as compared to volume excitations. The same comparison for a 2-keV electron in Cu is plotted in Fig. 9. Good agreement is found between present results (solid curve) and experimental data (dashed curve). Other model calculations provide poorer results at small energy losses.

Finally, we plot in Fig. 10 results of the REELS spectrum calculated presently (solid curve) and measured experimentally (dashed curve) (Ref. 4) for a 300-eV electron

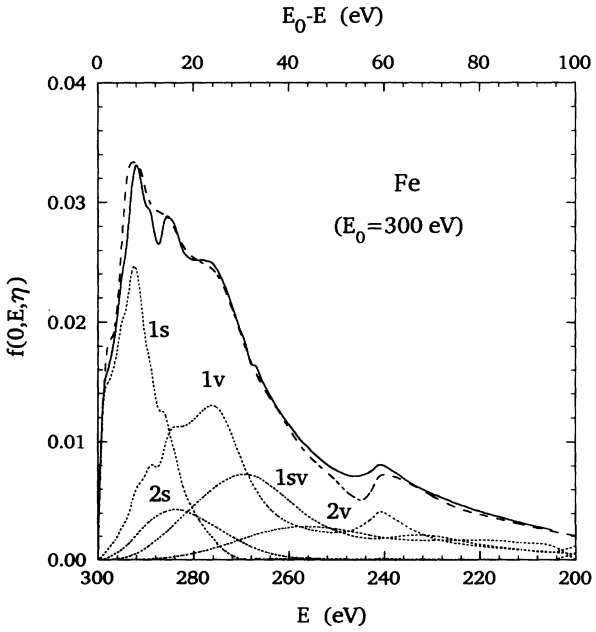

FIG. 10. A plot of the REELS spectrum for a 300-eV electron in Fe. The dashed, solid and dotted curves are, respectively, measured data (Ref. 4), present results, and individual contributions from surface- and volume-plasmon excitations.

in Fe. Good agreement is found over a wide range of energy losses. Individual contributions (dotted curves) from single and plural plasmon excitations are also plotted. Owing to the overlapping of these contributions, the gross REELS spectrum shows a broad peak with a full-width at half-maximum of about 30 eV.

IV. CONCLUSIONS

A theoretical model based on an improved dielectric function was used for calculations of the DIMFP for volume-plasmon excitations and the differential probability for surface-plasmon excitations under REELS conditions. In surface-plasmon calculations, we considered obliquely incident electrons with the recoil effect and without the small-scattering-angle assumption. For volume-plasmon excitations, we evaluated the corrections due to exchange and Z_1^3 effects. Results of these calculations were substituted into the transport equation to solve the energy and angular flux distribution of reflected electrons. Comparison between present results and experimental data for all calculated quantities showed close agreement to each other. It also showed that present results were better than other model calculations at, especially, small energy losses. Individual contributions to the REELS spectrum from single- and multiple-plasmon excitations were also analyzed. It revealed that the probability of plural surface-plasmon excitations was negligibly small for electrons with small incident angles.

Finally, it is noted that the present theory has treated elastic scatterings in Eqs. (23) and (25) using the P_1 approximation which assumed electron scatterings with isolated atoms randomly distributed in the solid. This assumption is only applicable to polycrystalline or amorphous solids where the Bragg diffraction is relatively weak.[1] The effect of Bragg diffraction takes into account the phase difference between waves scattered from each atom. For single crystals, this effect will focus the electron beam in a certain direction due to the periodic structure of these crystals. For polycrystalline or amorphous solids, the random elastic scatterings will apparently defocus the electron beam[46] so that the diffraction has little effect on electron-transport properties.

ACKNOWLEDGMENTS

This research was supported by the National Science Council of the Republic of China under Contract No. NSC83-0404-E-009-065.

[1]R. F. Egerton, *Electron Energy-Loss Spectroscopy in the Electron Microscope* (Plenum, New York, 1986).
[2]H. Raether, in *Excitations of Plasmons and Interband Transitions by Electrons,* edited by G. Höhler, Springer Tracts in Modern Physics Vol. 88 (Springer, New York, 1980).
[3]S. Tougaard and I. Chorkendorff, Phys. Rev. B **35**, 6570 (1987).
[4]S. Tougaard and J. Kraaer, Phys. Rev. B **43**, 1651 (1991).
[5]F. Yubero and S. Tougaard, Phys. Rev. B **46**, 2486 (1992).
[6]R. H. Ritchie, R. N. Hamm, J. E. Turner, H. A. Wright, and W. E. Bolch, in *Physical and Chemical Mechanisms in Molecular Radiation Biology,* edited by W. A. Glass and M. N. Varma (Plenum, New York, 1991), p. 99.
[7]M. Rosler, W. Brauer, J. Devooght, J. C. Dehaes, A. Dubus, M. Cailler, and J. P. Ganachaud, in *Particle Induced Electron Emission I,* edited by G. Höhler, Springer Tracts in Modern Physics Vol. 122 (Springer-Verlag, Berlin, 1991).
[8]J. C. Ashley and N. W. William, Radiat. Res. **81**, 364 (1980).
[9]M. Inokuti, Rev. Mod. Phys. **43**, 297 (1971).
[10]H. R. Philipp, in *Handbook of Optical Constants of Solids,* edited by E. D. Palik (Academic, London, 1985), p. 749.
[11]C. M. Kwei and C. J. Tung, J. Phys. D **19**, 255 (1986).
[12]D. Y. Smith and E. Shiles, Phys. Rev. B **17**, 4689 (1978).
[13]C. J. Tung and R. H. Ritchie, Phys. Rev. B **16**, 4302 (1977).
[14]N. F. Mott and H. S. W. Massey, *The Theory of Atomic Collisions,* 3rd ed. (Oxford University Press, Oxford, 1965).
[15]H. A. Bethe and R. W. Jackiw, *Intermediate Quantum Mechanics,* 3rd ed. (Benjamin Cummings, Menlo Park, CA, 1986).
[16]R. H. Ritchie, C. J. Tung, V. E. Anderson, and J. C. Ashley, Radiat. Res. **64**, 181 (1975).
[17]M. De Crescenzi, L. Lozzi, P. Picozzi, and S. Santucci, Phys. Rev. B **39**, 8409 (1989).
[18]J. C. Ashley, J. Phys. Condens. Matter **3**, 2741 (1991).
[19]J. M. Pitarke, R. H. Ritchie, and P. M. Echenique, Nucl. Instrum. Methods Phys. Res. Sect. B **79**, 209 (1993).
[20]J. D. Jackson and R. L. McCarthy, Phys. Rev. B **6**, 4131 (1972).
[21]J. C. Ashley, R. H. Ritchie, and W. Brandt, Phys. Rev. B **5**, 2393 (1972).
[22]J. J. Quinn, Phys. Rev. **126**, 1453 (1962).
[23]T. Fujikawa and L. Hedin, Phys. Rev. B **40**, 11 507 (1989).
[24]R. H. Ritchie, Phys. Rev. **106**, 874 (1957).
[25]B. Kunz, Z. Phys. **180**, 127 (1964).
[26]R. H. Ritchie and A. Howie, Philos. Mag. **36**, 463 (1977).
[27]R. H. Ritchie, R. N. Hamm, J. E. Turner, H. A. Wright, and W. E. Bolch, in *Physical and Chemical Mechanisms in Molecular Radiation Biology,* edited by W. A. Glass and M. N. Varma (Plenum, New York, 1991), p. 99.
[28]D. E. Aspnes, in *Handbook of Optical Constants of Solids,* edited by E. D. Palik (Academic, London, 1985), p. 89.
[29]C. V. Festenberg, Z. Phys. **227**, 453 (1969).
[30]J. C. Ashley, C. J. Tung, and R. H. Ritchie, Surf. Sci. **81**, 409 (1979).
[31]C. J. Tung, T. L. Chou, and C. M. Kwei, Radiat. Effects **59**, 7 (1981).
[32]W. R. Ferrell, R. H. Ritchie, and T. L. Ferrell, Am. J. Phys. **52**, 915 (1984).
[33]C. J. Tung, J. C. Ashley, and R. H. Ritchie, Surf. Sci. **81**, 427 (1979).
[34]C. J. Powell, Phys. Rev. **175**, 972 (1968).
[35]K. R. Kase and W. R. Nelson, *Concepts of Radiation Dosimetry* (Pergamon, Oxford, 1978).
[36]A. Tofterup, Phys. Rev. B **32**, 2808 (1985).
[37]R. H. Ritchie, C. J. Tung, V. E. Anderson, and J. C. Ashley, Radiat. Res. **64**, 181 (1975).
[38]M. A. Ordal, R. J. Bell, R. W. Alexander, L. L. Long, and M. R. Querry, Appl. Opt. **24**, 1985 (1985).
[39]T. J. Moravec, J. C. Rife, and D. L. Dexter, Phys. Rev. B **13**, 3297 (1976).
[40]P. B. Johnson and R. W. Christy, Phys. Rev. B **9**, 5056 (1974).

[41]R. C. Vehse, E. T. Arakawa, and M. W. Williams, Phys. Rev. B **1**, 517 (1970).
[42]D. L. Windt, W. C. Cash, Jr., M. Scott, P. Arendt, B. Newman, R. F. Fisher, and A. B. Swarzlander, Appl. Opt. **27**, 246 (1988).
[43]B. Dold and R. Mecke, Optik (Stuttgart) **22**, 435 (1965).
[44]H. J. Hagemann, W. Gudat, and C. Kunz, J. Opt. Soc. Am. **65**, 742 (1975).
[45]D. W. Lynch and W. R. Hunter, in *Handbook of Optical Constants of Solids I* (Ref. 28), p. 275.
[46]A. Jablonski, J. Gryko, J. Kraaer, and S. Tougaard, Phys. Rev. B **39**, 61 (1989).